Title

Peptide Spiders: Peptide–Polymer Conjugates to Traffic Nucleic Acids

Journal

Molecular Pharmaceutics, 17(9)

ISSN

1543-8384

Authors

Kwon, Ester J
Ko, Henry
Bhatia, Sangeeta N

Publication Date

2020-09-08

DOI

10.1021/acs.molpharmaceut.0c00714

Peer reviewed

HHS Public Access

Author manuscript

Mol Pharm. Author manuscript; available in PMC 2021 September 08.

Published in final edited form as:

Mol Pharm. 2020 September 08; 17(9): 3633–3642. doi:10.1021/acs.molpharmaceut.0c00714.

Peptide spiders: Peptide-polymer conjugates to traffic nucleic acids

Ester J. Kwon[a,b,1,*], **Henry Ko**[b,1], **Sangeeta N. Bhatia**[b,c,d,e,f,g,h,*]

[a]Current address: Department of Bioengineering, University of California San Diego, La Jolla, California 92093, USA

[b]Koch Institute for Integrative Cancer Research, Massachusetts Institute of Technology, Cambridge, Massachusetts 02139, USA

[c]Institute for Medical Engineering and Science, Massachusetts Institute of Technology, Cambridge, Massachusetts 02139, USA

[d]Department of Electrical and Computer Science, Massachusetts Institute of Technology, Cambridge, Massachusetts 02139, USA

[e]Marble Center for Cancer Nanomedicine, Massachusetts Institute of Technology, Cambridge, Massachusetts 02139, USA

[f]Department of Medicine, Brigham and Women's Hospital, Boston, Massachusetts 02115, USA

[g]Broad Institute of Massachusetts of Technology and Harvard, Cambridge, Massachusetts, 02139, USA

[h]Howard Hughes Medical Institute, Chevy Chase, Maryland 20815, USA

Abstract

Therapeutic nucleic acids hold great promise for treatment of genetic diseases, yet the delivery of this highly charged macromolecular drug remains a challenge in the field. Peptides are promising agents to mediate nucleic acid delivery because they can encode biological function to overcome the trafficking barriers. Electrostatic nanocomplexes of nucleic acid and peptides can achieve effective delivery, but the balance between their stability and biological function must be finely tuned. In this work, we explore two peptide building blocks that have been studied in the literature: targeting ligands and intracellular trafficking peptides. We grafted these peptides on a polyethylene glycol (PEG) backbone with eight sites for substitution to create so-called "peptide spiders". These conjugates achieve stability via the well-known hydrophilic shielding effect of PEG. In addition, the coordination of peptide building blocks into multimers may create new biological properties, such as the well-known phenomena of increased binding avidity with multivalent

[*]Corresponding authors: Department of Bioengineering, University of California San Diego, 9500 Gilman Drive MC 0412, La Jolla, California 92093, USA, ejkwon@ucsd.edu (E. J. Kwon).

[1]These author contributed equally

Conflicts of interest

There are no conflicts of interest to declare.

Data availability

The authors declare that all data supporting the findings of this study are available in the paper.

ligands. In this work, we linked two trafficking peptides to the PEG backbone using either non-reducible or reducible chemistries and investigated the ability of these materials to carry silencing RNAs into mammalian cells. We then investigated these nanomaterials for their pharmacokinetic properties and silencing of undruggable targets in a mouse model of cancer. While reducible linkages were more potent at silencing in vitro, this effect was reversed when applied in the context of living animals. This work offers a insight into peptide-based delivery materials and investigates peptide-polymer linkages.

Keywords

Peptides; polyethylene glycol; gene delivery; cancer

1. Introduction

The delivery of nucleic acids to specific cell types within the body offers a promising therapeutic avenue to regulate gene expression for the treatment of disease. Potential cargoes include nucleic acids to induce gene silencing (siRNA, miRNA), gene expression (mRNA transcripts, plasmid DNA), and CRISPR-based gene editing. To achieve nucleic acid delivery, the challenge is to chaperone a highly charged macromolecule so that it can navigate several biological hurdles including maintaining stability in the blood, extravasation into tissue, uptake in cells of interest, and intracellular trafficking to specific subcellular compartments. Nanoparticles offer a solution to address the challenges of nucleic acid delivery because they can be programmed with multiple functions into a single entity, such as protection and condensation of macromolecular cargo and trafficking through multi-scale biological barriers.[1,2] In addition, nanoparticles can assemble hundreds of molecules in an organized structure to create many advantages for drug delivery, for example hydrophobic pockets for drug loading, co-delivery of drug combinations, and creating high local concentrations for improvement of therapeutic indices. Inspired by viruses, a natural nanoparticle, engineers have incorporated biological function using biomolecules to achieve trafficking.[3] Beyond biological function, the pharmacokinetics of the nanoparticles must also be engineered and modern nanoparticle formulations incorporate molecules for stabilization; for example, ONPATTRO® is the first synthetic siRNA nanoparticle drug approved by the FDA and includes polyethylene glycol (PEG) in its formulation.[4]

One class of biomolecules is peptides, which are attractive candidates for clinical translation because they can display selective biological function while maintaining biocompatibility.[5] Their development as therapeutics has been facilitated by technology to improve their stability, including chemical modifications[6] or assembly on nanostructures.[7] Peptides have been used to transfer nucleic acid cargos into cells, in particular peptides that interact with membranes to overcome entrapment in endocytic vesicles.[8–10] Another class of peptides that has been studied widely across the nanoparticle field includes peptides that act as ligands to mediate active targeting.[11–13] In previous work, we described a peptide-based approach for siRNA delivery that combines both of these functional elements and includes a domain for (1) tumor-targeting/penetration and (2) endosomal escape that electrostatically assemble with nucleic acid cargo.[14,15] The result was a two component system comprised of nucleic

acid with trafficking peptide. Further refinements were made to this system to achieve stable vascular delivery, namely by exploring several architectures for the incorporation of polyethylene glycol (PEG) that preserved silencing activity.[16] This three component system was comprised of electrostatic complexation of nucleic acid with a trafficking peptide and peptide-PEG hybrid material. Both peptides and PEG have been widely investigated as components of nucleic acid delivery carriers,[17–19] and establishing strategies to engineer the structures of these materials has been an active area of research.[20–22] A remaining challenge is how to balance the seemingly conflicting goals of achieving stability in physiological solutions with the efficient cellular accumulation and release of cargo for successful delivery that presents a problem for many nonviral gene carriers when applied in vivo.[23–25] It is also the case that the incorporation strategy of PEG is dependent on the composition of the nanoparticle, and can include lipids, polymers, and metals.[26,27] Strategies to incorporate PEG into nanoparticles composed predominantly of peptides without compromising activity has yet to be resolved.[28,29]

In this work, we designed a nucleic acid carrier material that allows for stoichiometric control of two biological units: tumor-targeting and intracellular trafficking. In order to target tumors, we used iRGD, a peptide discovered via in vivo phage display that binds to upregulated $\alpha_v\beta_3$ integrins on tumor cells and stroma[30]. We and others have shown that iRGD modification can increase the accumulation of multiple nanoparticle types (e.g., liposomes, polymeric nanoparticles) into several tumor models[14,30–33]. We used transportan for intracellular trafficking, a membrane-active peptide that was identified in a screen of known cell penetrating peptides to increase intracellular delivery of siRNA cargo[15]. These biological units represented by peptides are coordinated on a multi-arm polyethylene glycol scaffold to promote stability of resulting nanoparticles after electrostatic complexation of nucleic acids. In addition, presentation of multimers of each biological unit has the potential to enhance biological function that is represented in nature. For example, multivalent targeting ligands are known to improve avidity[34,35] and mediate differential biological responses.[36] In another example, viral proteins that insert in membranes for transfer of genetic material or membrane rupture often have repeating subunits[37] or can work as multi-protein structures.[38,39] Synthetic peptides derived from these proteins have membrane-associating properties, and their arrangement in multimers can increase their activity.[40] To take advantage of these multimer effects, we arrange both targeting-targeting ligands and intracellular trafficking peptides as multimers in this work. Previous work has explored multi-valent peptides on polymer backbones,[41,42] although these studies were restricted to investigations in vitro; in the present work, we investigate the function of these materials in vivo. The challenge of predicting in vivo efficacy of non-viral gene carriers based on in vitro optimizations has been well-documented.[27,43] We investigated the role of attaching peptides with reducible or non-reducible bonds; although materials made with reducible disulfide bonds performed on par with those made with non-reducible bonds in *in vitro* silencing assays, materials with non-reducible bonds had improved performance when applied to animals bearing tumors. Overall, our work presents insights into the design principles of peptide-based electrostatic nucleic acid delivery nanoparticle, including a potential design for hydrophilic PEG stabilization and bond stability for the incorporation of trafficking peptides.

2. Materials and methods

2.1 Reagents

Peptides were synthesized by CPC Scientific to 90% purity. Transportan was synthesized with an N-terminal myristic acid and a C-terminal cysteine (myristic acid-GWTLNSAGYLLGKINLKALAALAKKILC) and iRGD was synthesized with an N-terminal azide (Azidoacetyl-GGGCRGDKGPDC). The following siRNA sequences were synthesized from Dharmacon: siLuc (CUUACGCUGAGUACUUCGA), siID4 (equimolar mixture of GCGAUAUGAACGACUGCUUAU and CCGACUUUAGAAGCCUACUUU). All fluorophore modified siRNA was prepared by modifying the 5' end on the sense strand. VivoTag-S-750 fluorophore was used for whole organ scans and siRNA encapsulation because this fluorophore is compatible with the LI-COR Odyssey imaging systems, DyLight 647 fluorophore was used for epifluorescence microscopy, and FAM fluorophore was used for immunohistochemistry because its signal can be amplified with antibody labeling.

2.2 Peptide spider conjugation

20,000 g/mol molecular weight 8-arm PEG was purchased functionalized with OPSS (Creative PEG Works) or maleimide (JenKem). The sizes of each PEG was verified by Matrix Assisted Laser Desorption/Ionization (MALDI) and found to be 14,000 g/mol and 20 g/mol, respectively. To prepare peptide conjugates, 8.1 equivalents of peptide at the indicated stoichiometry was added to PEG in dimethylformamide and 50 mM trimethylamine. After reaction for 4 hours in the dark, reaction was quenched with 100 mM cysteine for 15 minutes and dialyzed extensively into water using a 10,000 MWCO membrane for 4 complete exchanges.

2.3 Nanoparticle formulation and characterization

Conjugate concentrations were calculated based on the absorbance of the tryptophan residue in transportan at 280 nm and 6 transportan peptides per conjugate. For all in vitro studies, nanoparticles were formulated by adding equal volumes of conjugate to 2 μM siRNA in water at the indicated molar ratios and mixing rapidly. Nanoparticles were imaged with transmission electron microscopy by adsorbing particles to grids and negative stained with tungstophosphoric acid. Particles were imaged with a JEOL 2100 FEG TEM. Hydrodynamic diameters were measured using an 850 nm laser with a Wyatt Dyna Pro Plate Reader between 30 minutes at 6 hours after formulation of nanoparticles. Zeta potential measurements were made on a Malvern Zetasizer Nano. Nanoparticle concentration was measured with a Malvern NanoSight. For in vivo formulations, concentrations of conjugates and siRNA were ten-fold higher to create volumes suitable for in vivo administration.

2.4 Encapsulation Efficiency

Nanoparticles were formulated with VivoTag-S750-labeled siRNA at the indicated formulation ratios in triplicate. 6.7 pmoles of siRNA was loaded per lane of a 2% agarose gel and imaged on a LI-COR Odyssey. Amount of siRNA was quantified for each formulation normalized to a free siRNA control using ImageJ software to determine encapsulation efficiency.

2.5 Cell Culture

OVCAR-8 expressing firefly luciferase (OVCAR-8 Luc+) were a gift from Joyce Liu (Dana Farber Cancer Institute). U937 and MDA-MB-435S cells were obtained from ATCC. OVCAR-8 and U937 cells were cultured in RPMI 1640 media supplemented with 10% fetal bovine serum (FBS) and 1% penicillin & streptomycin (PS). MDA-MB-435S cells were cultured in Dulbecco's Modified Eagle's Medium supplemented with FBS and PS.

2.6 Silencing activity and toxicity

OVCAR-8 cells stably expressing luciferase were plated at 8,000 cells/well in a 96-well tissue culture plate 24 hours before transfection. Nanoparticles were formulated as described above with siLuc siRNA and added to cells in OptiMEM at less than 10% of the final volume. Cells were also transfected with Lipofectamine™ RNAiMAX (Invitrogen) according to manufacturer's instructions. Cells were incubated for 4 hours and medium was replaced with culture media for an additional 48 hours. Cell viability was measured by 3-(4,5-dimethylthiazol-2-yl)-5-(3-carboxymethoxyphenyl)-2-(4-sulfophenyl)-2H-tetrazolium) (MTS) using the CellTiter AQueous One Cell Proliferation Assay (Promega) according to manufacturer's instructions. Luciferase activity was measured by lysing cells with passive lysis buffer (Promega) and assaying 20 μL of lysate with 30 μL luciferin (Promega). Luminescence was integrated for 1 second on a Tecan Infinite M200 Pro plate reader and normalized by protein content measured by a bicinchoninic acid assay (Pierce).

2.7 Intracellular Distribution

OVCAR-8 cells were grown for 24 hours at ~50% confluency on coverglasses coated with 10 μg/mL poly-D-lysine. Cells were transfected as above at a final concentration of 100 nM Dy647-labeled siRNA formulated at a 4:1 ratio of peptide spider:siRNA and incubated at 37 °C for 2 hours. Cells were then rinsed with PBS twice and fixed in 4% paraformaldehyde. Cells were stained for lysosome-associated membrane protein-1 (LAMP1; Abcam) and counterstained with phalloidin and Hoechst (Invitrogen) and imaged on a Nikon Eclipse Ti microscope.

2.8 Cell association

Relative receptor expression was determined. U937 and MDA-MB-435S cells were harvested using Enzyme-free Cell Dissociation Buffer (Gibco) and incubated on ice for 15 minutes. Cells were blocked with 2% BSA, 10% donkey serum in PBS and cells were incubated with primary antibody against α_v integrin, $\alpha_v\beta_3$ integrin, or IgG control (BioLegend) for one hour. To measure nanoparticle association, cells were harvested as above and 100,000 cells per condition were incubated with nanoparticles formulated at a 4:1 ratio of peptide spider:siRNA with Dy547-labled siRNA at the indicated concentration for 2 hours on ice. After washing with PBS, cells were analyzed on a BD LSR Fortessa HTS and analyzed with FlowJo software.

2.9 Pharmacokinetics of nanoparticles in animals

A flank xenograft mouse model was created by bilaterally implanting $5–10\times10^6$ MDA-MB-435 cells subcutaneously in 4–5 week old female NCR-nude mice (Taconic).

Experiments were initiated when tumors had an average tumor volume between 200–300 mm^3 per flank. Mice were distributed to groups based on tumor size. To measure half-lives, nanoparticles formulated with 1 nmole of VivoTag-S 750-labeled siRNA at 4:1 ratio of peptide spider:siRNA in 5% dextrose were injected intravenously and 10 μL of blood was drawn at 0, 5, 15, 30, 60, and 120 minutes post injection. Biodistribution of nanoparticles in organs was determined by harvesting organs at 3 hours post injection and homogenizing samples in a hypotonic 1% SDS, 18 mM Tris, pH 7.4 buffer. Samples were then boiled and cleared before measuring fluorescence of VivoTag-S 750 in the tissue supernatant.

2.10 Imaging of nanoparticles in tumors

Tumors were implanted in mice as above and treated with nanoparticles prepared with 1 nmole of FAM-labeled siRNA at 4:1 ratio of peptide spider:siRNA injected at 24, 3, and 1 hour(s) prior to harvesting of tumors. Tumors were fixed with 4% paraformaldehyde and 10 μm frozen sections were prepared. FAM signal was amplified with the VectaFluor R.T.U. kit (Vector Laboratories) as per manufacturer's protocol. Sections were imaged on a Pannoramic 250 (3DHistech).

2.11 In vivo silencing activity

Nanoparticles were formulated at 4:1 ratio of peptide spider:siRNA using 2 nmoles of a 1:1 mixture of two ID4 siRNA sequences. Nanoparticles were injected intravenously in a 5% dextrose solution 6, 4, and 2 days before harvesting tumors. Tumors were frozen on dry ice and homogenized in lysis buffer supplemented with protease inhibitors. Western blot analysis was performed on lysates with antibody against ID4 (Abcam) and normalized by tubulin (Invitrogen). Quantification of protein was done by calculating area under the curve using ImageJ software.

2.12 Statistical Analysis

All statistical analysis was performed using GraphPad Prism software.

3. Results and Discussion

3.1 Synthesis and formulation of peptide spider nanoparticles

Peptide spiders were designed to display two trafficking peptides at the end of a polymer "leg" of an octo-valent polymer "body" (Figure 1A). Peptide spiders were synthesized by adding stoichiometric ratios of cysteine-terminated membrane-active transportan (GWTLNSAGYLLGKINLKALAALAKKILC) or tumor-penetrating ligand, iRGD (CRGDKGPDC), to 20,000 molecular weight 8-arm polyethylene glycol (PEG) linked via reducible orthopyridyl disulfide or non-reducible maleimide chemistries (Figure 1A). The targeting peptide, iRGD, was identified by in vivo phage display[30] and has been grafted onto many nanoparticle delivery systems for tumor targeting via binding $\alpha_v\beta_3$ integrin[44–46]. We have used transportan in previous work to improve endosomal escape of internalized cargo.[15,47] After synthesis, substitution of the materials was confirmed by MALDI to be between 60–80% reaction efficiency (Supplementary Data Figure 1). Concentrations of conjugate were calculated based on absorbance of tryptophans in the transportan peptide by UV-Vis spectroscopy and therefore all concentrations used in subsequent formulations were

standardized by the amount of transportan peptide. The resulting peptide spider conjugates were formulated into nanoparticles by adding equal volumes of conjugates to siRNA and mixing rapidly, as has been previously described for other electrostatic complexes.[48] The formation of spherical particles was confirmed by transmission electron microscopy (TEM) after negative staining with phosphotungstic acid (Figure 1A, Supplementary Figure S2). In order to confirm the diameters in aqueous solution as opposed to the dry conditions in TEM, we performed dynamic light scattering (DLS). Non-reducible or reducible peptide spider nanoparticles (PSNPs) were formulated at ratios of peptide:siRNA between 0.25 and 8, corresponding to N/P ratios between 0.156 and 5, as calculated from basic amino acids in transportan and phosphates in siRNA. The resulting hydrodynamic diameters were measured with DLS in water and in physiological levels of salt simulated by phosphate buffered saline (PBS) up to 6 hours after formulation, indicating that the nanoparticles were stable (Figure 1B). For PSNPs that formed nanoparticles, zeta potential measurements were made and surface potentials were found to be near neutral (Supplementary Data Figure 2). Encapulsation efficiency of siRNA was measured using a gel retardation assay, in which uncomplexed siRNA migrates into an agarose gel (Figure 1B). At conjugate to siRNA ratios above 2, when siRNA encapsulation was greater than 75%, both non-reducible and reducible peptide spider conjugates were able to form particles smaller than 100 nm in diameter. The measured hydrodynamic diameters of these particles were the same in water and in PBS, indicating that these particles were stable in physiological levels of salt. Peptide nanoparticles with no PEG when formulated at a ratio that fully encapsulated siRNA had diameters less than 100 nm but aggregated in the presence of PBS to have diameters larger than 1 micron, as observed previously.[16] We used a Malvern NanoSight to measure nanoparticle concentrations prepared at a 4:1 peptide conjugate:siRNA ratio and both non-reducible and reducible PSNPs formulations were measured to be ~5×10^8 nanoparticles/mL.

3.2 Silencing activity of peptide spider nanoparticles

Having established the ability to form nanoparticles with the peptide spider conjugates, a series of assays to evaluate function and trafficking within cells was completed. First, materials were evaluated in a reporter cell line stably expressing luciferase, OVCAR-8. Downregulation of luciferase enzyme as measured by luciferase activity normlzied by protein content (left axis) and cell viability (MTS assay, red diamonds; right axis) were measured 48 hours after treatment with nanoparticles formulated at peptide spider:siRNA ratios of 2, 4, and 8 and treated at a final siRNA concentration of 100 or 200 nM (Figure 2). 100% activity was determined by lysing untreated cells and measuring luciferase activity. All luminescence values were normalized by protein content as measured by bicinchoninic acid (BCA) assay to account for toxicity in addition to viability measurements with the MTS assay. As expected, free siRNA did not result in any silencing. The commercial reagent Lipofectamine RNAiMAX resulted in greater than 80% silencing, and was used to validate siRNA sequences *in vitro*. However, lipofectamine cannot be evaluated in systemic in vivo delivery due to the well-document toxicity of cationic liposomes.[49] Both non-reducible and reducible PSNPs were able to mediate ~ 50% silencing while maintaining viability above 80%. Based on titration of nanoparticle concentration and formulation ratios, reducible PSNPs appeared to be more effective at silencing compared to non-reducible PSNPs. All subsequent studies were performed with peptide spider:siRNA ratios of 4.

3.3 Intracellular distribution of peptide spider nanoparticles

Increased silencing activity, as observed for reducible PSNPs, may be attributable to several factors. One hypothesis is differential intracellular trafficking of cargo. To test this hypothesis, OVCAR-8 cells were imaged by microscopy after internalization of nanoparticles prepared with fluorescently labeled siRNA. PSNPs were incubated at 37 °C with cells for 2 hours, washed, and fixed in triplicate. Once nanoparticles are internalized into cells, they are typically found in endosomes, and if they cannot escape into the cytosol, endosomes will mature into lysosomes.[50] Cells were labeled for lysosomes (lysosomal-associated membrane protein 1 (LAMP1)), filamental actin (phalloidin), and nuclei (Hoechst) and imaged by microscopy (Figure 3). As expected, no siRNA signal was detected in untreated cells. Comparison of siRNA distribution after delivery with non-reducible and reducible peptide spiders reveals that both materials are able to enter cells, but that reducible PSNPs lead to diffuse cytosolic siRNA with few puncta compared to the appearance of distinctly punctate siRNA signal in non-reducible PSNP-treated cells (Figure 3, insets). This observation suggests that linkage of peptides through reducible disulfide bonds leads to increased endosomal escape of cargo siRNA. It is also possible that the diffuse versus punctate appearance of siRNA is due to more stable complexation in nanoparticles made with non-reducible compared to reducible polymers. Based on glutathione levels measured in endocytic vesicles[51], peptides could separate from the PEG polymer backbone in peptide spiders made with reducible bonds, leading to the subsequent release of siRNA cargo and a more diffuse appearance.

3.4 Cell-association of peptide spider nanoparticles in cells with low and high receptor expression

The discrepancy in the efficacy of silencing by non-reducible versus reducible PSNPs might also be due to differential association of material with cells. Increased association of nanoparticles can yield increased silencing activity, as elevated concentrations of siRNA nanoparticles can enhance silencing activity, as observed when cells are incubated with PSNPs at a final siRNA concentration of 200 nM (Figure 2). To investigate the association of PSNPs with cells, two cell lines with low and high expression of the iRGD receptors were employed for binding studies. The cognate receptors for iRGD are integrin heterodimers, most prominently $\alpha_v\beta_3/\beta_5$ integrins.[30] Two human cancer cell lines were evaluated for their receptor expression by flow cytometry; U937, a human lymphoma cell line, expresses low levels of $\alpha_v\beta_3$ and α_v while MDA-MB-435S, a human melanoma cell line, expresses high levels of both (Figure 4A). Non-reducible and reducible PSNPs were formulated with fluorescently-labeled siRNA at a peptide spider:siRNA ratio of 4 and incubated with cells at the indicated concentrations for 1 hour at 4 °C. Cells were pre-chilled to 4 °C to inhibit internalization machinery within cells.[52] After removal of free nanoparticles with washing, signal of fluorescently-labeled siRNA was quantified with flow cytometry. Both non-reducible and reducible PSNPs had increased signal in integrin-high MDA-MB-435 cells over integrin-low U937 cells (Figure 4B). Furthermore, based on this analysis, reducible PSNPs had increased fluorescence signal with cells compared with non-reducible PSNPs, which may have contributed, at least partly, to the increased silencing activity observed when cells were treated with reducible PSNPs (Figure 2). Although it was not expected that reducible PSNPs would have more associated fluorescence signal with cells compared to

non-reducible PSNPs, it may be due to the differences in the sizes of the 8-arm PEG backbones which were synthesized by two different vendors. Although both reducible and non-reducible backbones were purchased at 20 kDa sizes for comparison, when the materials were characterized by Matrix Assisted Laser Desorption/Ionization (MALDI) they were measured to be 14 KDa for PEG with reducible linkages and 20 KDa for PEG with non-reducible linkages. We do not believe the 30% difference in backbone size is responsible for the markedly different intracellular distributions (Figure 3) since they formed similarly sized nanoparticles (Figure 1B). We also note that at 100 nM concentration of siRNA, total binding is similar between reducible and non-reducible PSNPs (Figure 4), and both the transfection and imaging study were conducted at this concentration of siRNA or higher (Figures 2 and 3).

3.5 Pharmacokinetics of peptide spider nanoparticle accumulation in tumor model

Having established that peptide spiders were able to form nanoparticles that exhibit silencing activity, we applied them to a mouse model of cancer. Using the MDA-MB-435S cell line that expresses a high level of integrin (Figure 3A), tumor cells were implanted subcutaneously into both flanks of nude mice. Once the resulting tumors reached 200–300 mm^3 in volume, studies were conducted. Nanoparticles were formulated at 4:1 ratio of peptide spider:siRNA at a 10 μM final siRNA concentration, 10-fold higher than what was used in vitro, in order to obtain volumes suitable for in vivo administration. Hydrodynamic diameters were measured at this concentration, since it is known that formulation concentration affects particle sizes. Diameters of PSNP formulated at 10 μM were ~100 nm, moderately bigger than those measured at 1 μM final siRNA concentration used for in vitro studies (Figure 1B) but diameters were still reasonable for systemic vascular delivery. By contrast, peptide without PEG formed particles with diameters >1 μm when formulated at high 10 μM concentrations compared to the ~80 nm diameters when formulated at 1 μM concentrations (Figure 1B). Previous reports in the literature have shown that the diameters of nanoparticles formed by electrostatic self assembly are concentration dependent[53,54]. Although it is unknown whether the large, micron-scaled particles formed using peptide without PEG are due to particle formation or rapid aggregation, the introduction of PEG improved the formulation of nanoparticles with small hydrodynamic diameters suitable for intravenous application. In physiological levels of salt simulated by PBS, both non-reducible and reducible PSNPs maintained diameters ~100 nm, similar sizes formed in water (Figure 5A). Nanoparticles were administered to mice at a 1 nmole dose via the tail vein, and blood half-life was measured by sampling 10 μL of blood for a period of 2 hours (Figure 5B). Half-lives were on the order of minutes for all nanoparticles; half-lives were 1.8 min for peptide NPs, 2.1 min for NR-PSNPs, and 3.6 min for R-PSNPs. Three hours after administration of nanoparticles, mice were sacrificed and the tumors, heart, lung, liver, kidney, and spleen were dissected and processed to create tissue lysates. Fluorescence signal of VivoTag-S 750-labeled siRNA was measured in the supernatant (Figure 5C–D). A slight increase in material was detected in tumors from mice that received PSNPs compared to peptide nanoparticles, although it was not statistically significant (Figure 5C). The observation that active targeting may not significantly affect bulk biodistribution, but is critical for cell-specific interaction and/or retention in the tissue, has been observed consistently in the literature[55–57]. Consistent with what has been observed with large particle

accumulation in organs of the reticuloendothelial system (RES)[58], PSNPs had less accumulation in off-target organs compared to nanoparticles made with no PEG (Figure 5D). In particular, non-reducible PSNPs had significantly less accumulation in the lung and kidney, relative to peptide nanoparticles. However, it is noted that there is significant off-target organ accumulation of the PSNPs[59]. Similarly, PEG lipid nanoparticles that are the basis for the only FDA-approved siRNA drug Onpattro are observed to accumulate in the liver and spleen[4,60] and reducing off-target organ accumulation for tumor delivery remains an outstanding challenge for the field.

3.6 Tissue distribution of peptide spider nanoparticles in tumors

The accumulation of materials within the tumor tissue were investigated by administering PSNPs made with 1 nmole of FAM-labeled siRNA at 24, 3, and 1 hour(s) before harvesting of tumors (Figure 6). Tumors were sectioned and the FAM label amplified using immunolabeling. Relative levels of siRNA detected in the tumor by non-reducible PSNPs was higher than peptide nanoparticles and reducible PSNPs. Furthermore, reducible PSNP-delivered siRNA appeared to be restricted in tissue areas compared to a more distributed appearance of non-reducible PSNP-delivered siRNA. This relative difference may be attributed to reduction of the linkage and subsequent dissociation of trafficking peptides from the PEG backbone in the biological environment of the blood or tumor tissue.

3.7 Activity of peptide spider nanoparticles in tumor models

Lastly, we looked at the ability of our PSNP system to downregulate target proteins. To do this, we formulated nanoparticles with siRNA against the transcription factor ID4, known to be upregulated in tumors[14], and administered 2 nmoles of siRNA per dose (or 1.4 mg/kg) at 6, 4, and 2 days before harvesting tissue. Past reports on systemically-delivered peptide-based delivery systems for siRNA in the literature have been administered at siRNA doses between 0.5 and 1.7 mg/kg[61–64]. We first looked at toxicity of these materials under the conditions of repeat dosing. The heart, lung, liver, kidney, and spleen were embedded in paraffin and stained with hematoxylin and eosin. A pathologist blinded to the conditions of the mice inspected the tissue and found no signs of toxicity in any tissue. Representative images of triplicate samples are presented in Figure 7. The knockdown of the target protein ID4 was analyzed in tumor lysates using Western blotting (Figure 8A). Non-reducible PSNPs were able to mediate ~60% downregulation of ID4 protein, whereas reducible PSNPs mediated ~30% downregulation and non-PEGylated peptide nanoparticles did not mediate significant downregulation in this dosing scheme. These results were unexpected because reducible PSNPs outperformed non-reducible PSNPs when evaluated in vitro. However, there are multiple trafficking barriers that occur before nanoparticles reach their target cells (e.g., blood protein interactions, off-target organ accumulation, and tissue extravasation), which cannot be predicted by culture model systems. We hypothesized that reduction of the linkage keeping peptides on the PEG backbone could cause destabilization of reducible PSNPs before they could reach their target destination either in the blood or the tumor microenvironment. To test this prediction, we incubated non-reducible and reducible PSNPs with the reducing agent dithiothreitol (DTT) at 5 mM in PBS and monitored their hydrodynamic diameters over time (Figure 8B). Whereas non-reducible PSNPs were unaffected by treatment with DTT as expected, reducible PSNPs had increasing diameters

over time, indicating removal of the PEG shielding and particle aggregation (Figure 8C). The nanoparticle aggregation of reducible PSNPs may have contributed to the decreased silencing activity observed (Figure 8A). The aggregation of reducible PSNPs prior to reaching tumors cells is also supported by the appearance of concentrated siRNA signal in tumors compared to the diffuse siRNA signal in tumors after non-reducible PSNP delivery (Figure 6). Our observations are in contrast to other reducible siRNA delivery systems in the literature that achieve robust silencing[65–67]. In our system, transportan peptide is required for both intracellular release and siRNA binding through the multiple cationic amino acid residues. Therefore, reduction of the disulfide bond separates the siRNA binding component from PEG, which is required for stability of the nanoparticles. In previous examples of reducible systems, disulfide bonds were used to stabilize siRNA to siRNA interactions[66] or attach endosomal escape components with siRNA binding/stabilizing components[65]. Other factors that may contribute to differences in stability of various disulfide crosslinked nanoparticles that still require further investigation are the relative stability of the nanoparticles themselves, the number of disulfide crosslinks, the local chemical environment of the disulfide bonds, and the steric shielding of the disulfide bonds.[68]

4. Conclusions

In this work, we engineered a material to deliver nucleic acids using a polymeric backbone grafted with trafficking peptides. We investigated the stability of the linker used to attach peptides to the polymeric backbone and found that although a reducible linker can lead to more efficient delivery in cultured cells, a non-reducible linker was more effective at functional delivery to tumors in animal models. This finding highlights the need for holistic consideration of trafficking barriers in the design of systemically-delivered nucleic acid carriers, where optimal design criteria between intracellular and systemic delivery may be conflicting. In one well-documented example of the need to balance design criteria of gene carriers intended for systemic delivery, PEG is added to FDA-approved nanoparticle formulations in order to improve pharmacokinetics[69] even though it is known that PEG reduces gene silencing activity[43]. Alternatively, the advantage of reducible bonds to confer silencing activity could be capitalized through local delivery, such as intratumoral injection; intratumoral injection is a particularly promising route of administration for immunotherapy[70,71]. In summary, this work offers insight into the stability of peptide-polymer hybrid materials for use in nucleic acid delivery.

Supplementary Material

Refer to Web version on PubMed Central for supplementary material.

Acknowledgments

The authors thank Dr. Heather Fleming (MIT) for critical reading of the manuscript. We thank the Koch Institute Swanson Biotechnology Core at MIT. This study was supported in part by a Koch Institute Support Grant P30-CA14051 from the National Cancer Institute (Swanson Biotechnology Center), a Core Center Grant P30-ES002109 from the National Institute of Environmental Health Sciences, the Ludwig Fund for Cancer Research, and the Koch Institute Marble Center for Cancer Nanomedicine. E.J.K. acknowledges funding from the NIH (F32CA177094). S.N.B is a Howard Hughes Medical Institute Investigator.

References

(1). Yin H; Kanasty RL; Eltoukhy AA; Vegas AJ; Dorkin JR; Anderson DG Non-Viral Vectors for Gene-Based Therapy. Nat. Rev. Genet 2014, 15 (8), 541–555. 10.1038/nrg3763. [PubMed: 25022906]

(2). Richner JM; Himansu S; Dowd KA; Butler SL; Salazar V; Fox JM; Julander JG; Tang WW; Shresta S; Pierson TC; Ciaramella G; Diamond MS Modified MRNA Vaccines Protect against Zika Virus Infection. Cell 2017, 168 (6), 1114–1125.e10. 10.1016/j.cell.2017.02.017. [PubMed: 28222903]

(3). Davis ME; Zuckerman JE; Choi CHJ; Seligson D; Tolcher A; Alabi CA; Yen Y; Heidel JD; Ribas A Evidence of RNAi in Humans from Systemically Administered SiRNA via Targeted Nanoparticles. Nature 2010, 464 (7291), 1067–1070. 10.1038/nature08956. [PubMed: 20305636]

(4). Akinc A; Maier MA; Manoharan M; Fitzgerald K; Jayaraman M; Barros S; Ansell S; Du X; Hope MJ; Madden TD; Mui BL; Semple SC; Tam YK; Ciufolini M; Witzigmann D; Kulkarni JA; Meel R. van der; Cullis PR The Onpattro Story and the Clinical Translation of Nanomedicines Containing Nucleic Acid-Based Drugs. Nat. Nanotechnol 2019, 14 (12), 1084–1087. 10.1038/s41565-019-0591-y. [PubMed: 31802031]

(5). Fosgerau K; Hoffmann T Peptide Therapeutics: Current Status and Future Directions. Drug Discov. Today 2015, 20 (1), 122–128. 10.1016/j.drudis.2014.10.003. [PubMed: 25450771]

(6). Walensky LD; Bird GH Hydrocarbon-Stapled Peptides: Principles, Practice, and Progress. J. Med. Chem 2014, 57 (15), 6275–6288. 10.1021/jm4011675. [PubMed: 24601557]

(7). Sheridan C Proof of concept for next-generation nanoparticle drugs in humans https://www.nature.com/articles/nbt0612-471 (accessed Mar 12, 2018). 10.1038/nbt0612-471.

(8). Endoh T; Ohtsuki T Cellular SiRNA Delivery Using Cell-Penetrating Peptides Modified for Endosomal Escape. Adv. Drug Deliv. Rev 2009, 61 (9), 704–709. 10.1016/j.addr.2009.04.005. [PubMed: 19383521]

(9). Eguchi A; Meade BR; Chang Y-C; Fredrickson CT; Willert K; Puri N; Dowdy SF Efficient SiRNA Delivery into Primary Cells by a Peptide Transduction Domain–DsRNA Binding Domain Fusion Protein. Nat. Biotechnol 2009, 27 (6), 567–571. 10.1038/nbt.1541. [PubMed: 19448630]

(10). Whitehead KA; Langer R; Anderson DG Knocking down Barriers: Advances in SiRNA Delivery. Nat. Rev. Drug Discov 2009, 8 (2), 129–138. 10.1038/nrd2742. [PubMed: 19180106]

(11). Ruoslahti E; Bhatia SN; Sailor MJ Targeting of Drugs and Nanoparticles to Tumors. J. Cell Biol 2010, 188 (6), 759–768. 10.1083/jcb.200910104. [PubMed: 20231381]

(12). McCarthy JR; Weissleder R Multifunctional Magnetic Nanoparticles for Targeted Imaging and Therapy. Adv. Drug Deliv. Rev 2008, 60 (11), 1241–1251. 10.1016/j.addr.2008.03.014. [PubMed: 18508157]

(13). Byrne JD; Betancourt T; Brannon-Peppas L Active Targeting Schemes for Nanoparticle Systems in Cancer Therapeutics. Adv. Drug Deliv. Rev 2008, 60 (15), 1615–1626. 10.1016/j.addr.2008.08.005. [PubMed: 18840489]

(14). Ren Y; Cheung HW; Maltzhan G. von; Agrawal A; Cowley GS; Weir BA; Boehm JS; Tamayo P; Karst AM; Liu JF; Hirsch MS; Mesirov JP; Drapkin R; Root DE; Lo J; Fogal V; Ruoslahti E; Hahn WC; Bhatia SN Targeted Tumor-Penetrating SiRNA Nanocomplexes for Credentialing the Ovarian Cancer Oncogene ID4. Sci. Transl. Med 2012, 4 (147), 147ra112–147ra112. 10.1126/scitranslmed.3003778.

(15). Ren Y; Hauert S; Lo JH; Bhatia SN Identification and Characterization of Receptor-Specific Peptides for SiRNA Delivery. ACS Nano 2012, 6 (10), 8620–8631. 10.1021/nn301975s. [PubMed: 22909216]

(16). Lo JH; Kwon EJ; Zhang AQ; Singhal P; Bhatia SN Comparison of Modular PEG Incorporation Strategies for Stabilization of Peptide–SiRNA Nanocomplexes. Bioconjug. Chem 2016, 27 (10), 2323–2331. 10.1021/acs.bioconjchem.6b00304. [PubMed: 27583545]

(17). Bolhassani A Potential Efficacy of Cell-Penetrating Peptides for Nucleic Acid and Drug Delivery in Cancer. Biochim. Biophys. Acta 2011, 1816 (2), 232–246. 10.1016/j.bbcan.2011.07.006. [PubMed: 21840374]

(18). Nakase I; Akita H; Kogure K; Gräslund A; Langel U; Harashima H; Futaki S Efficient Intracellular Delivery of Nucleic Acid Pharmaceuticals Using Cell-Penetrating Peptides. Acc. Chem. Res 2012, 45 (7), 1132–1139. 10.1021/ar200256e. [PubMed: 22208383]

(19). Lehto T; Ezzat K; Wood MJA; EL Andaloussi S Peptides for Nucleic Acid Delivery. Adv. Drug Deliv. Rev 2016, 106, 172–182. 10.1016/j.addr.2016.06.008. [PubMed: 27349594]

(20). Lächelt U; Wagner E Nucleic Acid Therapeutics Using Polyplexes: A Journey of 50 Years (and Beyond). Chem. Rev 2015, 115 (19), 11043–11078. 10.1021/cr5006793. [PubMed: 25872804]

(21). Tan J-KY; Sellers DL; Pham B; Pun SH; Horner PJ Non-Viral Nucleic Acid Delivery Strategies to the Central Nervous System. Front. Mol. Neurosci 2016, 9. 10.3389/fnmol.2016.00108.

(22). Vlerken L. E. van; Vyas TK; Amiji MM Poly(Ethylene Glycol)-Modified Nanocarriers for Tumor-Targeted and Intracellular Delivery. Pharm. Res 2007, 24 (8), 1405–1414. 10.1007/s11095-007-9284-6. [PubMed: 17393074]

(23). Mishra S; Webster P; Davis ME PEGylation Significantly Affects Cellular Uptake and Intracellular Trafficking of Non-Viral Gene Delivery Particles. Eur. J. Cell Biol 2004, 83 (3), 97–111. 10.1078/0171-9335-00363. [PubMed: 15202568]

(24). Hatakeyama H; Akita H; Harashima H The Polyethyleneglycol Dilemma: Advantage and Disadvantage of PEGylation of Liposomes for Systemic Genes and Nucleic Acids Delivery to Tumors. Biol. Pharm. Bull 2013, 36 (6), 892–899. 10.1248/bpb.b13-00059. [PubMed: 23727912]

(25). Jackson MA; Bedingfield SK; Yu F; Stokan ME; Miles RE; Curvino EJ; Hoogenboezem EN; Bonami RH; Patel SS; Kendall PL; Giorgio TD; Duvall CL Dual Carrier-Cargo Hydrophobization and Charge Ratio Optimization Improve the Systemic Circulation and Safety of Zwitterionic Nano-Polyplexes. Biomaterials 2019, 192, 245–259. 10.1016/j.biomaterials.2018.11.010. [PubMed: 30458360]

(26). Suk JS; Xu Q; Kim N; Hanes J; Ensign LM PEGylation as a Strategy for Improving Nanoparticle-Based Drug and Gene Delivery. Adv. Drug Deliv. Rev 2016, 99, 28–51. 10.1016/j.addr.2015.09.012. [PubMed: 26456916]

(27). Werfel TA; Jackson MA; Kavanaugh TE; Kirkbride KC; Miteva M; Giorgio TD; Duvall C Combinatorial Optimization of PEG Architecture and Hydrophobic Content Improves Ternary SiRNA Polyplex Stability, Pharmacokinetics, and Potency in Vivo. J. Controlled Release 2017, 255, 12–26. 10.1016/j.jconrel.2017.03.389.

(28). Deshayes S; Morris M; Heitz F; Divita G Delivery of Proteins and Nucleic Acids Using a Non-Covalent Peptide-Based Strategy. Adv. Drug Deliv. Rev 2008, 60 (4), 537–547. 10.1016/j.addr.2007.09.005. [PubMed: 18037526]

(29). He D; Wagner E Defined Polymeric Materials for Gene Delivery. Macromol. Biosci 2015, 15 (5), 600–612. 10.1002/mabi.201400524. [PubMed: 25655078]

(30). Sugahara KN; Teesalu T; Karmali PP; Kotamraju VR; Agemy L; Girard OM; Hanahan D; Mattrey RF; Ruoslahti E Tissue-Penetrating Delivery of Compounds and Nanoparticles into Tumors. Cancer Cell 2009, 16 (6), 510–520. 10.1016/j.ccr.2009.10.013. [PubMed: 19962669]

(31). Sugahara KN; Teesalu T; Karmali PP; Kotamraju VR; Agemy L; Greenwald DR; Ruoslahti E Coadministration of a Tumor-Penetrating Peptide Enhances the Efficacy of Cancer Drugs. Science 2010, 328 (5981), 1031–1035. 10.1126/science.1183057. [PubMed: 20378772]

(32). Gu G; Gao X; Hu Q; Kang T; Liu Z; Jiang M; Miao D; Song Q; Yao L; Tu Y; Pang Z; Chen H; Jiang X; Chen J The Influence of the Penetrating Peptide IRGD on the Effect of Paclitaxel-Loaded MT1-AF7p-Conjugated Nanoparticles on Glioma Cells. Biomaterials 2013, 34 (21), 5138–5148. 10.1016/j.biomaterials.2013.03.036. [PubMed: 23582684]

(33). Yan F; Wu H; Liu H; Deng Z; Liu H; Duan W; Liu X; Zheng H Molecular Imaging-Guided Photothermal/Photodynamic Therapy against Tumor by IRGD-Modified Indocyanine Green Nanoparticles. J. Controlled Release 2016, 224, 217–228. 10.1016/j.jconrel.2015.12.050.

(34). Weissleder R; Kelly K; Sun EY; Shtatland T; Josephson L Cell-Specific Targeting of Nanoparticles by Multivalent Attachment of Small Molecules. Nat. Biotechnol 2005, 23 (11), 1418–1423. 10.1038/nbt1159. [PubMed: 16244656]

(35). Hammarström S Binding of Helix Pomatia A Hemagglutinin to Human Erythrocytes and Their Cells. Influence of Multivalent Interaction on Affinity. Scand. J. Immunol 1973, 2 (1), 53–66. 10.1111/j.1365-3083.1973.tb02016.x. [PubMed: 4728059]

(36). Collins BE; Paulson JC Cell Surface Biology Mediated by Low Affinity Multivalent Protein-Glycan Interactions. Curr. Opin. Chem. Biol 2004, 8 (6), 617–625. 10.1016/j.cbpa.2004.10.004. [PubMed: 15556405]

(37). Skehel JJ; Wiley DC Receptor Binding and Membrane Fusion in Virus Entry: The Influenza Hemagglutinin. Annu. Rev. Biochem 2000, 69, 531–569. 10.1146/annurev.biochem.69.1.531. [PubMed: 10966468]

(38). Lindwasser OW; Resh MD Multimerization of Human Immunodeficiency Virus Type 1 Gag Promotes Its Localization to Barges, Raft-Like Membrane Microdomains. J. Virol 2001, 75 (17), 7913–7924. 10.1128/JVI.75.17.7913-7924.2001. [PubMed: 11483736]

(39). Maldarelli F; Chen MY; Willey RL; Strebel K Human Immunodeficiency Virus Type 1 Vpu Protein Is an Oligomeric Type I Integral Membrane Protein. J. Virol 1993, 67 (8), 5056–5061. [PubMed: 8331740]

(40). Kim H; Kitamatsu M; Ohtsuki T Enhanced Intracellular Peptide Delivery by Multivalent Cell-Penetrating Peptide with Bioreducible Linkage. Bioorg. Med. Chem. Lett 2018, 28 (3), 378–381. 10.1016/j.bmcl.2017.12.035. [PubMed: 29275934]

(41). Zeng H; Little HC; Tiambeng TN; Williams GA; Guan Z Multifunctional Dendronized Peptide Polymer Platform for Safe and Effective SiRNA Delivery. J. Am. Chem. Soc 2013, 135 (13), 4962–4965. 10.1021/ja400986u. [PubMed: 23496091]

(42). Imani R; Prakash S; Vali H; Faghihi S Polyethylene Glycol and Octa-Arginine Dual-Functionalized Nanographene Oxide: An Optimization for Efficient Nucleic Acid Delivery. Biomater. Sci 2018, 6 (6), 1636–1650. 10.1039/C8BM00058A. [PubMed: 29757340]

(43). Kanasty R; Dorkin JR; Vegas A; Anderson D Delivery Materials for SiRNA Therapeutics. Nat. Mater 2013, 12 (11), 967–977. 10.1038/nmat3765. [PubMed: 24150415]

(44). Chow EK-H; Ho D Cancer Nanomedicine: From Drug Delivery to Imaging. Sci. Transl. Med 2013, 5 (216), 216rv4–216rv4. 10.1126/scitranslmed.3005872.

(45). Peng Z-H; Kopeček J Enhancing Accumulation and Penetration of HPMA Copolymer–Doxorubicin Conjugates in 2D and 3D Prostate Cancer Cells via IRGD Conjugation with an MMP-2 Cleavable Spacer. J. Am. Chem. Soc 2015, 137 (21), 6726–6729. 10.1021/jacs.5b00922. [PubMed: 25963409]

(46). Zhou J; Patel TR; Fu M; Bertram JP; Saltzman WM Octa-Functional PLGA Nanoparticles for Targeted and Efficient SiRNA Delivery to Tumors. Biomaterials 2012, 33 (2), 583–591. 10.1016/j.biomaterials.2011.09.061. [PubMed: 22014944]

(47). Kwon EJ; Skalak M; Lo Bu R; Bhatia SN Neuron-Targeted Nanoparticle for SiRNA Delivery to Traumatic Brain Injuries. ACS Nano 2016, 10 (8), 7926–7933. 10.1021/acsnano.6b03858. [PubMed: 27429164]

(48). Pun SH; Bellocq NC; Liu A; Jensen G; Machemer T; Quijano E; Schluep T; Wen S; Engler H; Heidel J; Davis ME Cyclodextrin-Modified Polyethylenimine Polymers for Gene Delivery. Bioconjug. Chem 2004, 15 (4), 831–840. 10.1021/bc049891g. [PubMed: 15264871]

(49). Lv H; Zhang S; Wang B; Cui S; Yan J Toxicity of Cationic Lipids and Cationic Polymers in Gene Delivery. J. Controlled Release 2006, 114 (1), 100–109. 10.1016/j.jconrel.2006.04.014.

(50). Sahay G; Querbes W; Alabi C; Eltoukhy A; Sarkar S; Zurenko C; Karagiannis E; Love K; Chen D; Zoncu R; Buganim Y; Schroeder A; Langer R; Anderson DG Efficiency of SiRNA Delivery by Lipid Nanoparticles Is Limited by Endocytic Recycling. Nat. Biotechnol 2013, 31 (7), 653–658. 10.1038/nbt.2614. [PubMed: 23792629]

(51). Jiang X; Yu Y; Chen J; Zhao M; Chen H; Song X; Matzuk AJ; Carroll SL; Tan X; Sizovs A; Cheng N; Wang MC; Wang J Quantitative Imaging of Glutathione in Live Cells Using a Reversible Reaction-Based Ratiometric Fluorescent Probe. ACS Chem. Biol 2015, 10 (3), 864–874. 10.1021/cb500986w. [PubMed: 25531746]

(52). Beisiegel U; Schneider WJ; Goldstein JL; Anderson RG; Brown MS Monoclonal Antibodies to the Low Density Lipoprotein Receptor as Probes for Study of Receptor-Mediated Endocytosis and the Genetics of Familial Hypercholesterolemia. J. Biol. Chem 1981, 256 (22), 11923–11931. [PubMed: 6271765]

(53). Grzelczak M; Vermant J; Furst EM; Liz-Marzán LM Directed Self-Assembly of Nanoparticles. ACS Nano 2010, 4 (7), 3591–3605. 10.1021/nn100869j. [PubMed: 20568710]

(54). Romøren K; Pedersen S; Smistad G; Evensen Ø; Thu BJ The Influence of Formulation Variables on in Vitro Transfection Efficiency and Physicochemical Properties of Chitosan-Based Polyplexes. Int. J. Pharm 2003, 261 (1), 115–127. 10.1016/S0378-5173(03)00301-6. [PubMed: 12878400]

(55). Choi CHJ; Alabi CA; Webster P; Davis ME Mechanism of Active Targeting in Solid Tumors with Transferrin-Containing Gold Nanoparticles. Proc. Natl. Acad. Sci. U. S. A 2010, 107 (3), 1235–1240. 10.1073/pnas.0914140107. [PubMed: 20080552]

(56). Bartlett DW; Su H; Hildebrandt IJ; Weber WA; Davis ME Impact of Tumor-Specific Targeting on the Biodistribution and Efficacy of SiRNA Nanoparticles Measured by Multimodality in Vivo Imaging. Proc. Natl. Acad. Sci 2007, 104 (39), 15549–15554. 10.1073/pnas.0707461104. [PubMed: 17875985]

(57). Wang J; Lee GY; Lu Q; Peng X; Wu J; Wu S; Kairdolf BA; Nie S; Wang Y; Lane LA Quantitative Examination of the Active Targeting Effect: The Key Factor for Maximal Tumor Accumulation and Retention of Short-Circulated Biopolymeric Nanocarriers. Bioconjug. Chem 2017, 28 (5), 1351–1355. 10.1021/acs.bioconjchem.7b00138. [PubMed: 28448116]

(58). Jiang W; Kim BYS; Rutka JT; Chan WCW Nanoparticle-Mediated Cellular Response Is Size-Dependent. Nat. Nanotechnol 2008, 3 (3), 145–150. 10.1038/nnano.2008.30. [PubMed: 18654486]

(59). Wilhelm S; Tavares AJ; Dai Q; Ohta S; Audet J; Dvorak HF; Chan WCW. Analysis of Nanoparticle Delivery to Tumours. Nat. Rev. Mater 2016, 1 (5), 16014. 10.1038/natrevmats.2016.14.

(60). Mui BL; Tam YK; Jayaraman M; Ansell SM; Du X; Tam YYC; Lin PJ; Chen S; Narayanannair JK; Rajeev KG; Manoharan M; Akinc A; Maier MA; Cullis P; Madden TD; Hope MJ Influence of Polyethylene Glycol Lipid Desorption Rates on Pharmacokinetics and Pharmacodynamics of SiRNA Lipid Nanoparticles. Mol. Ther. - Nucleic Acids 2013, 2, e139. 10.1038/mtna.2013.66. [PubMed: 24345865]

(61). Boisguérin P; Deshayes S; Gait MJ; O'Donovan L; Godfrey C; Betts CA; Wood MJA; Lebleu B Delivery of Therapeutic Oligonucleotides with Cell Penetrating Peptides. Adv. Drug Deliv. Rev 2015, 87, 52–67. 10.1016/j.addr.2015.02.008. [PubMed: 25747758]

(62). Crombez L; Morris MC; Dufort S; Aldrian-Herrada G; Nguyen Q; Mc Master G; Coll J-L; Heitz F; Divita G Targeting Cyclin B1 through Peptide-Based Delivery of SiRNA Prevents Tumour Growth. Nucleic Acids Res. 2009, 37 (14), 4559–4569. 10.1093/nar/gkp451. [PubMed: 19483097]

(63). Michiue H; Eguchi A; Scadeng M; Dowdy SF Induction of in Vivo Synthetic Lethal RNAi Responses to Treat Glioblastoma. Cancer Biol. Ther 2009, 8 (23), 2304–2311. 10.4161/cbt.8.23.10271.

(64). Hou KK; Pan H; Ratner L; Schlesinger PH; Wickline SA Mechanisms of Nanoparticle-Mediated SiRNA Transfection by Melittin-Derived Peptides. ACS Nano 2013, 7 (10), 8605–8615. 10.1021/nn403311c. [PubMed: 24053333]

(65). Li J; Cheng D; Yin T; Chen W; Lin Y; Chen J; Li R; Shuai X Copolymer of Poly(Ethylene Glycol) and Poly(L-Lysine) Grafting Polyethylenimine through a Reducible Disulfide Linkage for SiRNA Delivery. Nanoscale 2014, 6 (3), 1732–1740. 10.1039/C3NR05024F. [PubMed: 24346086]

(66). Lee SJ; Yook S; Yhee JY; Yoon HY; Kim M-G; Ku SH; Kim SH; Park JH; Jeong JH; Kwon IC; Lee S; Lee H; Kim K Co-Delivery of VEGF and Bcl-2 Dual-Targeted SiRNA Polymer Using a Single Nanoparticle for Synergistic Anti-Cancer Effects in Vivo. J. Controlled Release 2015, 220, 631–641. 10.1016/j.jconrel.2015.08.032.

(67). Zhou Z; Li H; Wang K; Guo Q; Li C; Jiang H; Hu Y; Oupicky D; Sun M Bioreducible Cross-Linked Hyaluronic Acid/Calcium Phosphate Hybrid Nanoparticles for Specific Delivery of SiRNA in Melanoma Tumor Therapy. ACS Appl. Mater. Interfaces 2017, 9 (17), 14576–14589. 10.1021/acsami.6b15347. [PubMed: 28393529]

(68). Oupický D; Li J Bioreducible Polycations in Nucleic Acid Delivery: Past, Present, and Future Trends. Macromol. Biosci 2014, 14 (7), 908–922. 10.1002/mabi.201400061. [PubMed: 24678057]

(69). Garber K Alnylam launches era of RNAi drugs https://www.nature.com/articles/nbt0918-777 (accessed Jan 2, 2020). 10.1038/nbt0918-777.

(70). Aznar MA; Tinari N; Rullán AJ; Sánchez-Paulete AR; Rodriguez-Ruiz ME; Melero I Intratumoral Delivery of Immunotherapy—Act Locally, Think Globally. J. Immunol 2017, 198 (1), 31–39. 10.4049/jimmunol.1601145. [PubMed: 27994166]

(71). Wang S; Campos J; Gallotta M; Gong M; Crain C; Naik E; Coffman RL; Guiducci C Intratumoral Injection of a CpG Oligonucleotide Reverts Resistance to PD-1 Blockade by Expanding Multifunctional CD8+ T Cells. Proc. Natl. Acad. Sci 2016, 113 (46), E7240–E7249. 10.1073/pnas.1608555113. [PubMed: 27799536]

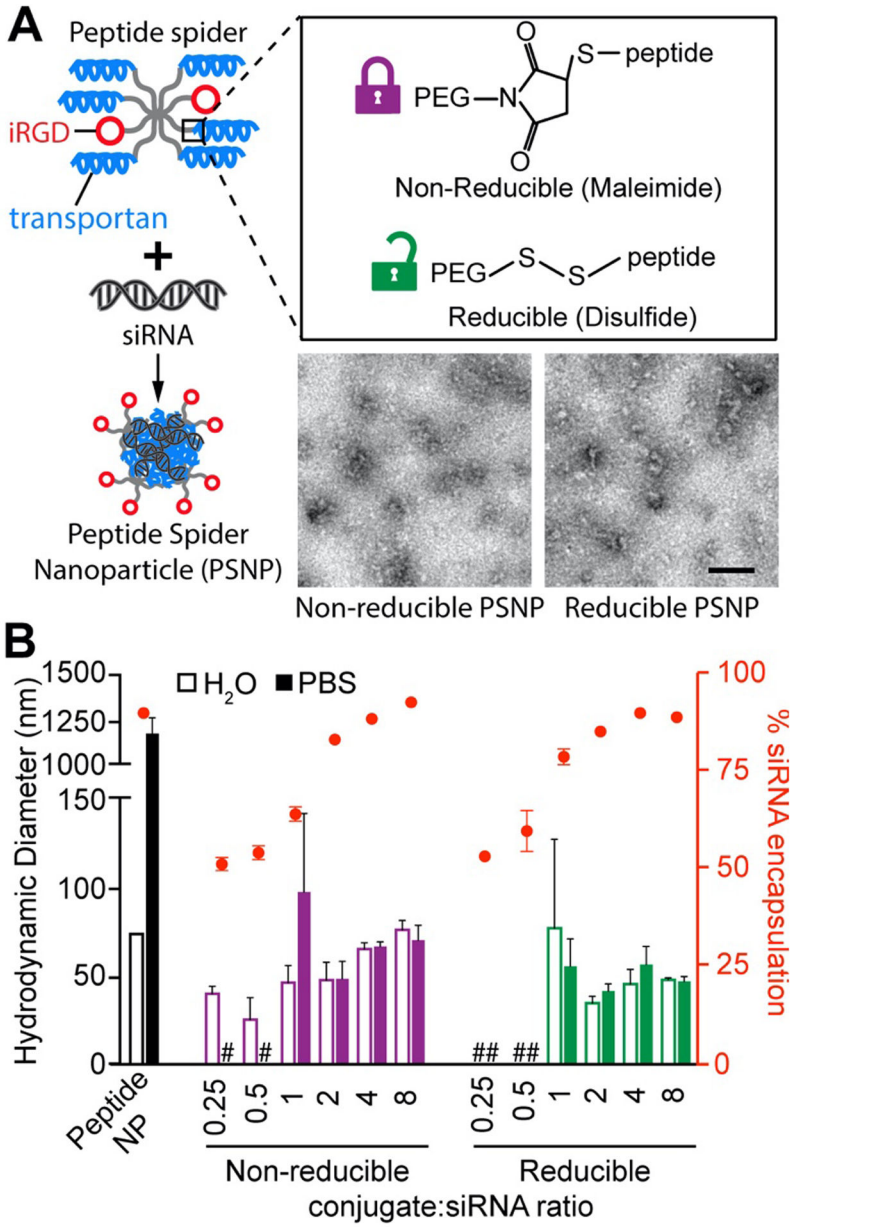

Figure 1. Design of peptide spider nanoparticles.

(A) Schematic of a peptide spider. 8-arm polyethylene glycol is modified with trafficking peptides via non-reducible/reducible linkages and can condense siRNA. Transmission electron microscopy of nanoparticles formed with peptide spider conjugates reveal spherical nanoparticles (scale bar = 100 nm). (B) Hydrodynamic diameters measured by dynamic light scattering in water (empty bars) or PBS (solid bars). Diameters that could not be measured due to poor particle formation are denoted by a #. Percent siRNA encapsulation of corresponding nanoparticles denoted by red circles (right y-axis; n=3, mean +SD).

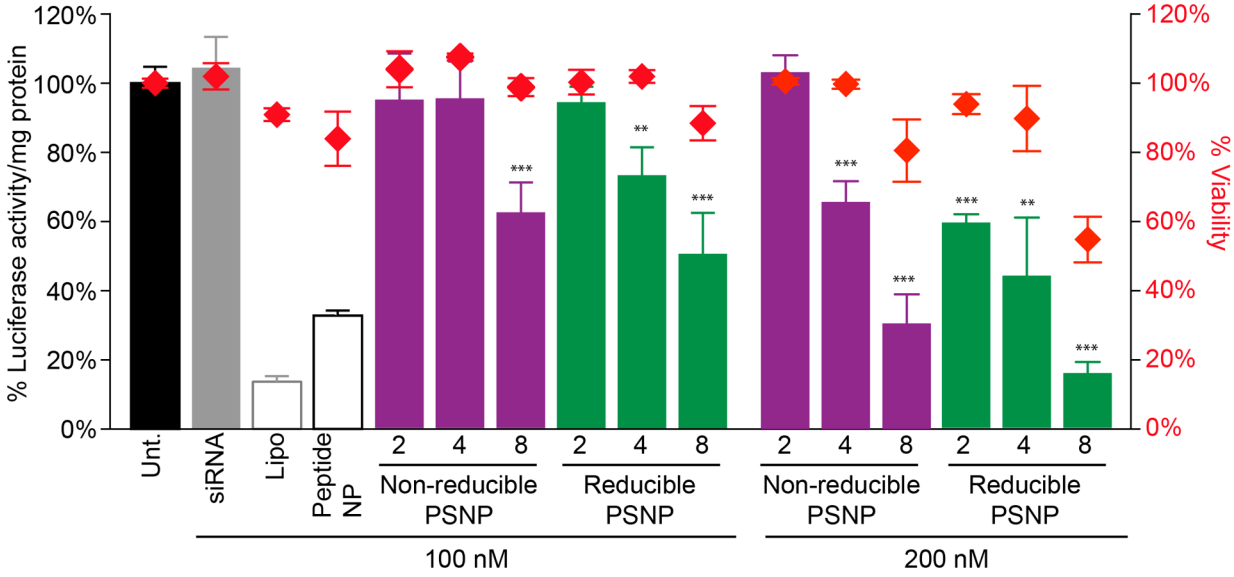

Figure 2. Silencing activity of peptide spiders.

Non-reducible and reducible peptide spider nanoparticles carrying siRNA against luciferase formulated at 2, 4, and 8 conjugate:siRNA ratios were delivered to a reporter cell line stably expressing luciferase. Luciferase activity normalized by protein content (left y-axis; bars) and cell viability assayed by MTS (right y-axis; red diamonds) were measured 48 hours after treatment with nanoparticles (n=3, mean ±SD). Controls included untreated cells, free siRNA, commercial reagent Lipofectamine RNAiMAX, and peptide nanoparticles. (**p<0.01, ***p<0.001 One-way ANOVA with Dunnett's post test).

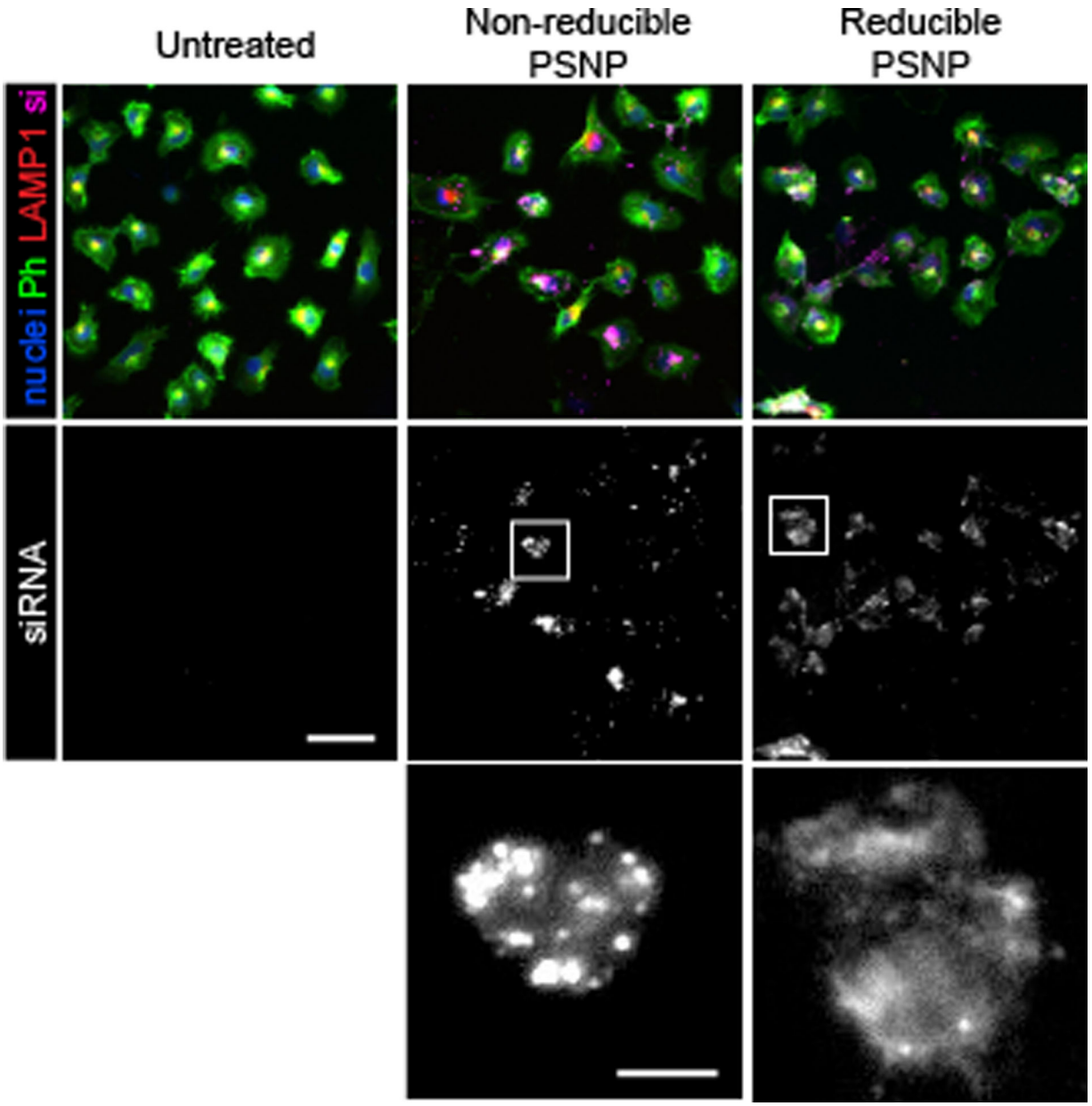

Figure 3. Intracellular distribution of peptide spider nanoparticles.

Cells were incubated with non-reducible and reducible peptide spider nanoparticles (PSNP) carrying fluorescently labeled siRNA (Cy5; magenta) for 2 hours and fixed and stained. Cells were imaged for nuclei (Hoechst; blue), microtubules (Phalloidin; green), and lysosomes (LAMP1; red) using microscopy (scale bar = 50 mm). Bottom row shows enlargement of white box in siRNA image (scale bar = 10 mm; representative images from n=3 study; study repeated in independent experiments).

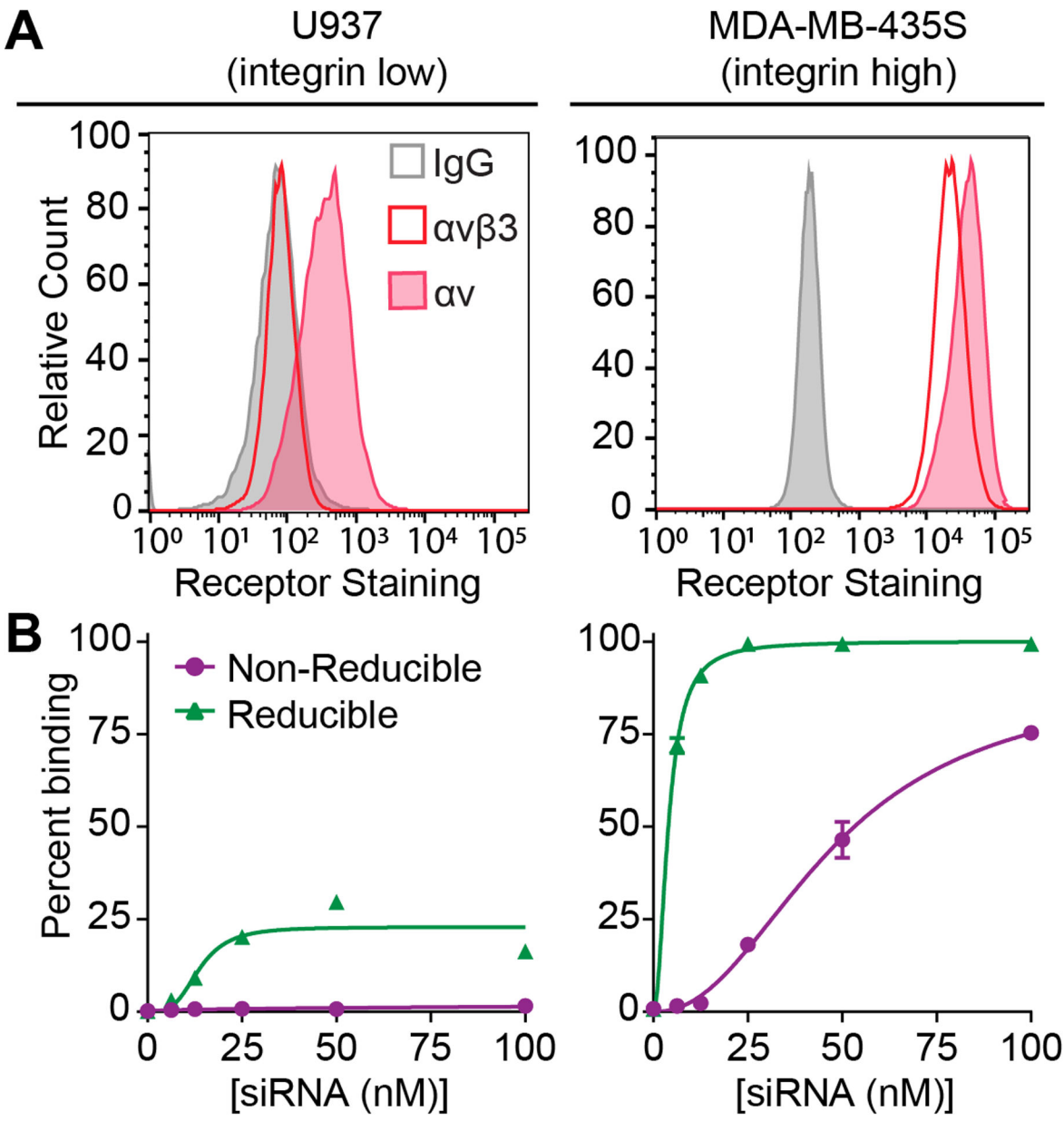

Figure 4. Cell association of peptide spider nanoparticles.

(A) U937 and MDA-MB-435S cell lines were characterized for α_v and $\alpha_v\beta_3$ integrin staining using flow cytometry. (B) Association of non-reducible and reducible peptide spider nanoparticles carrying fluorescently labeled siRNA with U937 cells (left) or MDA-MB-435S cells (right) at several concentrations (n=3, mean ±SD).

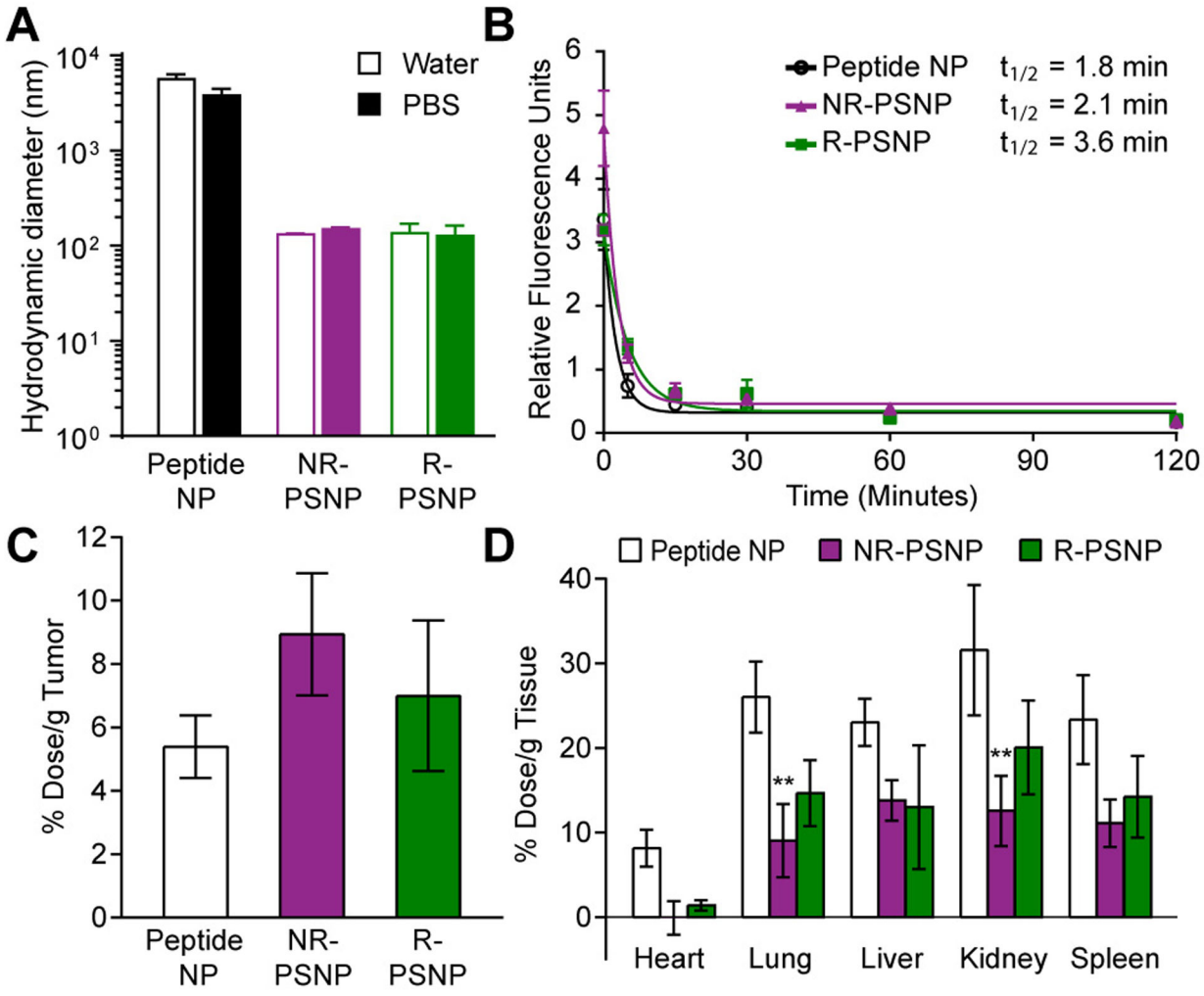

Figure 5. Pharmacokinetics of peptide spider nanoparticles.

(A) Sizes of non-reducible and reducible peptide spider nanoparticles measured by dynamic light scattering made at high concentrations (10 μM) suitable for in vivo injections. (B) Blood half-life of non-reducible and reducible PSNPs after intravenous delivery in mice (n=3, mean ±SEM). Measurement of PSNPs carrying fluorescently labeled siRNA in (C) tumors and (D) organs 3 hours after intravenous administration in mice bearing subcutaneous tumors (n=3, mean ±SEM). (**p<0.01 2-way ANOVA with Tukey's post test.)

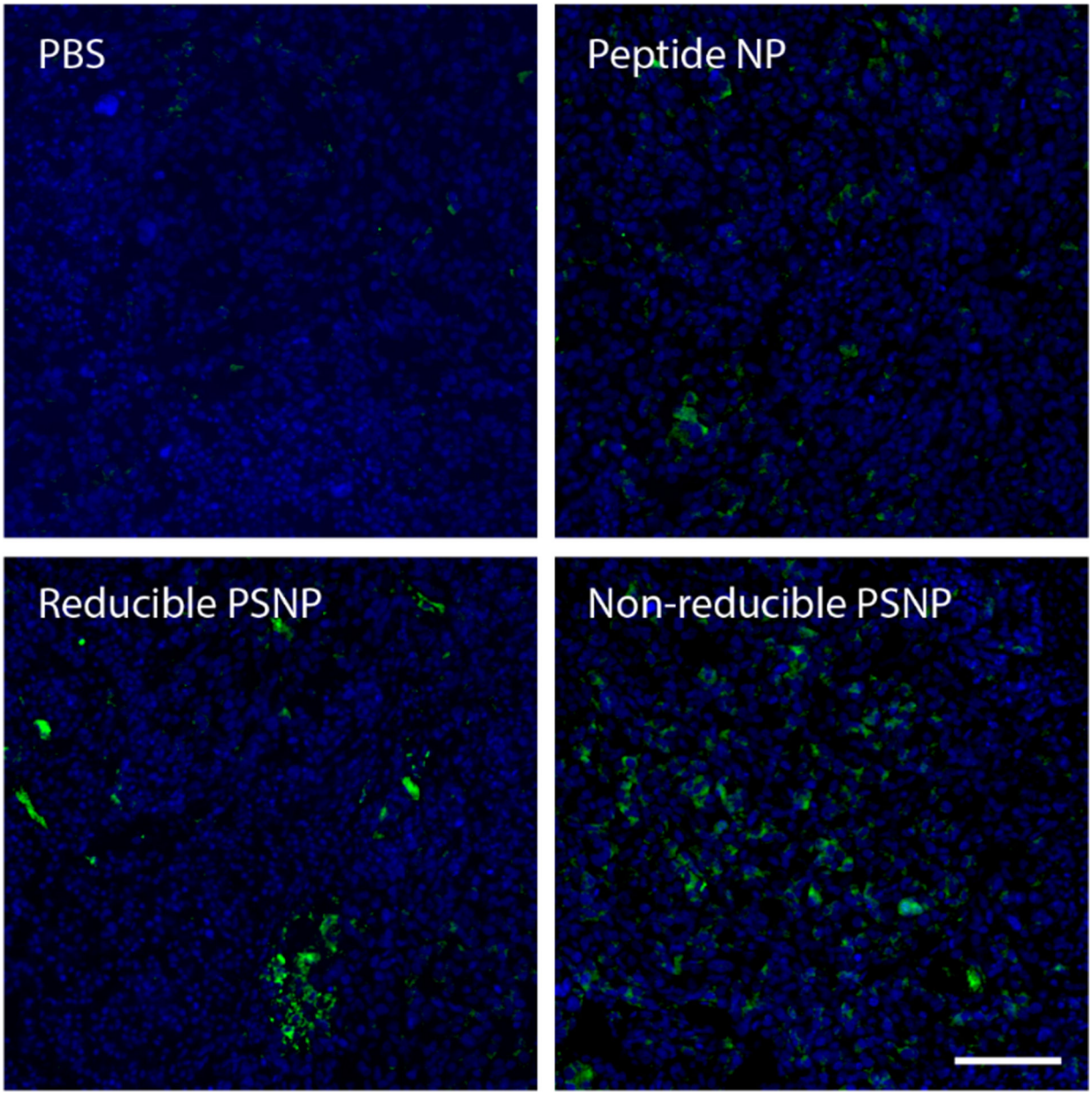

Figure 6. Tissue distribution of PSNP in tumor tissue.

Mice were dosed with 1 nmole of FAM-labeled siRNA dosed at 24, 3, and 1 hour(s) before tumors were excised. Tumors were sectioned and siRNA signal was amplified using immunolabeling (green) and sections counterstained for nuclei (Hoechst; blue). Representative areas of the tumor are shown (n=3–4 tumors per condition, scale bar = 100 μm).

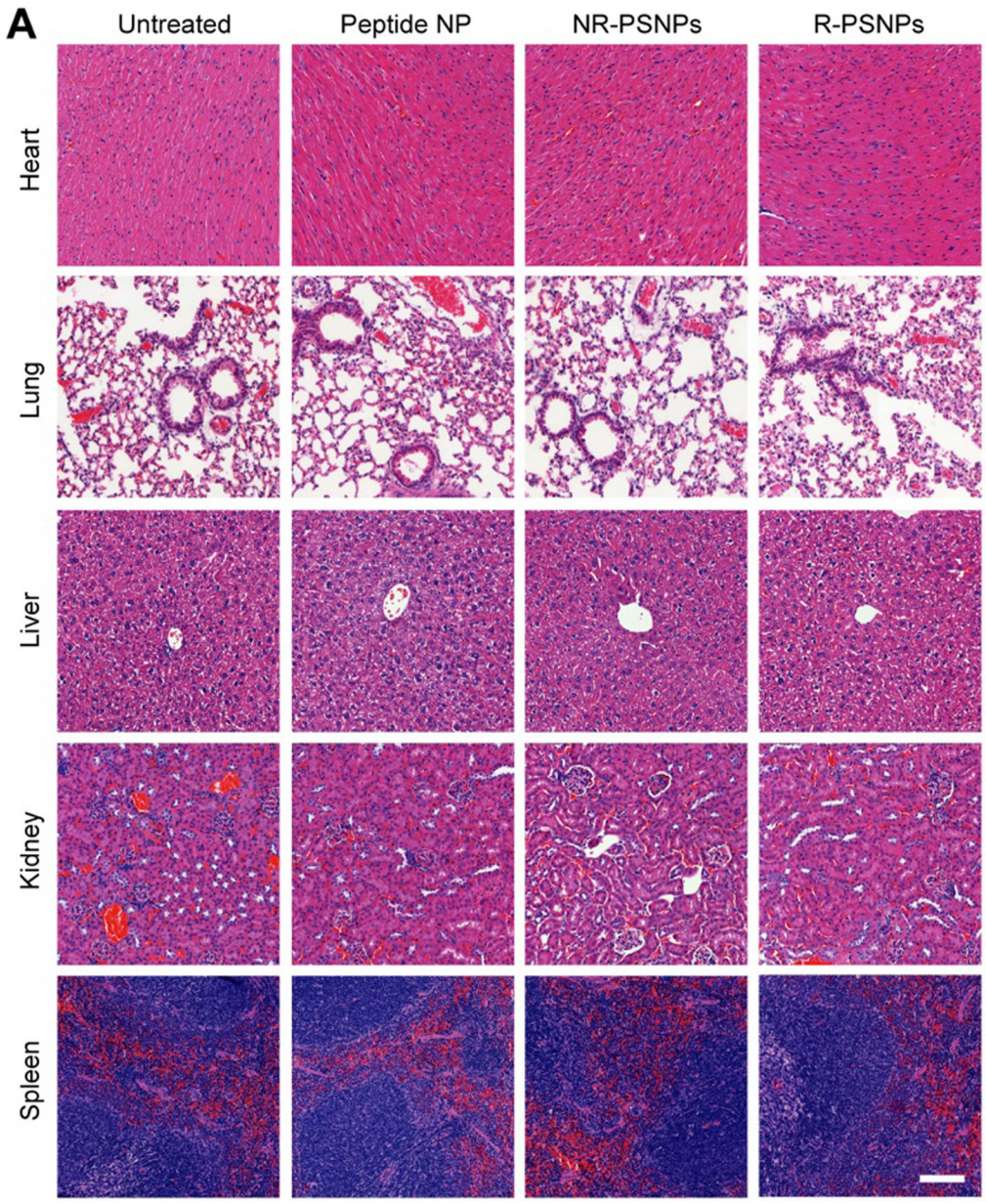

Figure 7. Toxicity of peptide spider nanoparticles.

Hematoxylin and eosin staining of heart, lung, liver, kidney, and spleen from mice administered 3 doses of nanoparticles (scale bar = 100 μm; n=3, representative images shown).

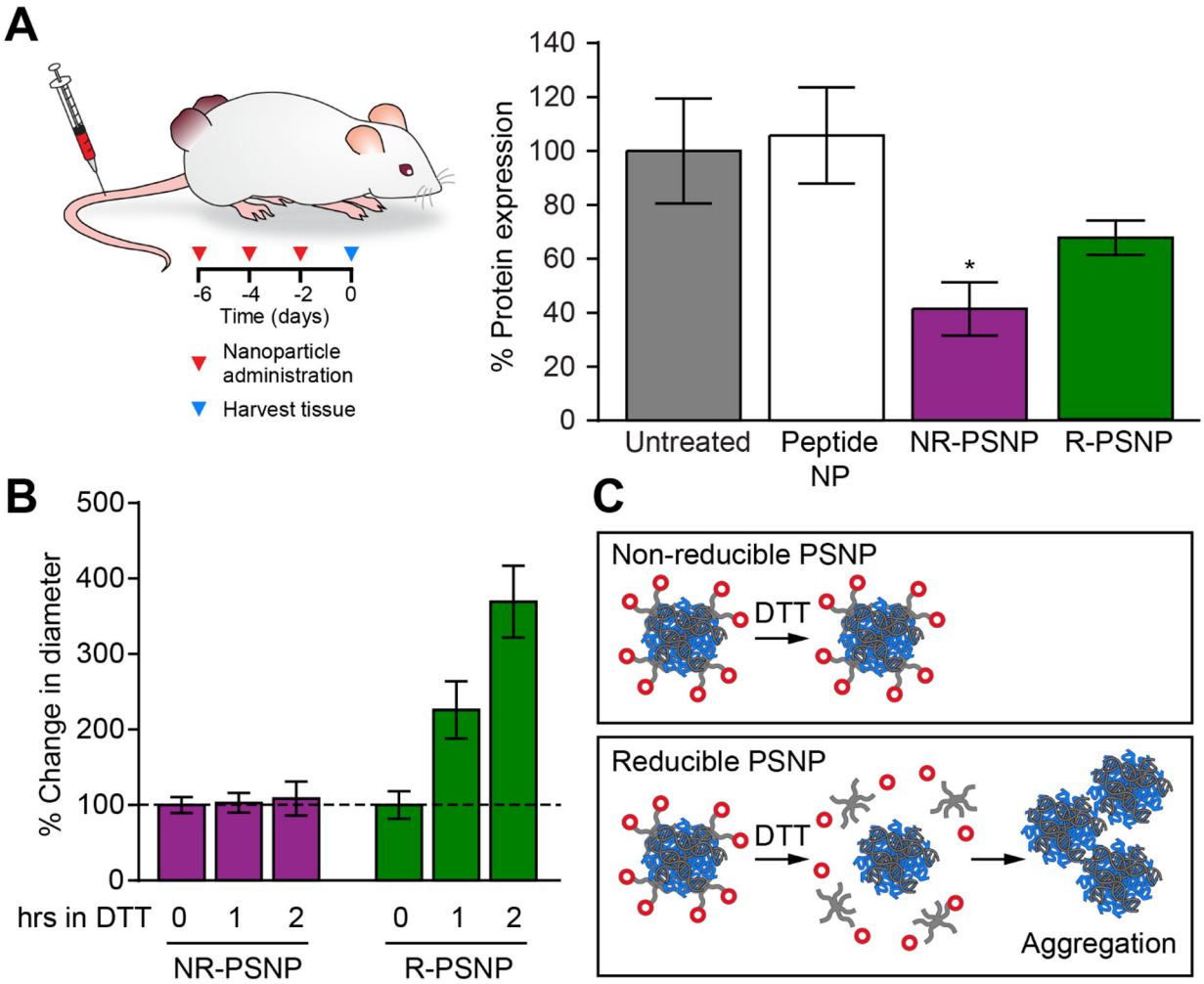

Figure 8. Silencing efficacy of peptide spider nanoparticles in vivo.

(A) Time line of nanoparticle administration. Right, ID4 protein knockdown in flank model of MDA-MB-435S tumors after treatment with non-reducible or reducible peptide spider nanoparticles (n=4, mean ±SEM, *p<0.05 one-way ANOVA with Dunnett's post test.) (B) Changes in hydrodynamic diameters of PSNPs from time 0 after treatment with the reducing agent, DTT at 5 mM (n=3, mean ±SD). (C) Schematic of proposed mechanism of DTT initiated aggregation.